13th World Conference on Earthquake Engineering
Vancouver, B.C., Canada
August 1-6, 2004
Paper No. 446

3-D FINITE ELEMENT CYCLIC ANALYSIS OF RC BEAM/COLUMN JOINT USING SPECIAL BOND MODEL

Kazuki TAJIMA[1], Takamichi MISHIMA[2], Nobuaki SHIRAI[3]

SUMMARY

Nonlinear finite element analyses on the RC beam-column joint specimens failing in shear tested under cyclic lateral loading were conducted to investigate their failure modes and post peak behaviors such as cyclic deterioration and shear resistance mechanism. The analyses were performed especially by paying attention to spatial discretization (2-D or 3-D), modeling of bond behavior (bond-slip model or bond locking model) and type of loading (monotonic or cyclic). Consequently, 2-D analysis with bond slip model gives comparable story shear-story drift angle relation to the one obtained under the monotonic loading condition. However, it provides different hysteresis loop from the one observed in the test under the cyclic loading condition. On the other hand, 3-D analysis with bond-locking model is able to reproduce cyclic deterioration and hysteresis loop after the peak load fairly well. It seems that 3-D analysis gives better representation of the failure mode than 2-D analysis. Furthermore, a macroscopic model for predicting the joint capacity proposed by Shiohara is reviewed and validity of his hypotheses is rigorously investigated through comparison of the observed and calculated results.

INTRODUCTION

Beam-column joint assemblage in the RC moment-resisting framed structures is a critical seismic element because its behavior under severe earthquake motions has a significant effect on failure mode and strength and deformation capacity of the building structures. Thus, many experimental studies have been conducted to understand failure and resistant mechanisms of the beam-column joints so far.

Concerning shear failure of the joint, the current seismic codes [1][2][3] provides the upper limit of input shear to the joint; that is, degradation of the story shear and localization of the shear deformation to the joint. Permissible limit of the input shear is expressed by a simple empirical formula in terms of the compressive strength of concrete. On the other hand, Kitayama et al. [4] conducted the cyclic lateral loading test on the interior beam-column joint specimens with different bond properties of longitudinal rebars in the beam through the joint. In addition, the earthquake response analyses by the simplified framed model were performed using two kind of hysteresis models; one is a regular Takeda model and the

[1] Nihon University, Japan, k.tajima@rc.arch.cst.nihon-u.ac.jp
[2] Shimizu Corporation, Japan, takamichi_mishima@shimz.co.jp
[3] Nihon University, Japan, shirai@arch.cst.nihon-u.ac.jp

other is a modified Takeda model characterized by a significant effect of the bond slip on a shape of the hysteresis loop. Consequently, they derived several recommendations on the limitation by the so-called bond index indicating bond deterioration of rebars, the limitation of the ratio of rebar diameter in the beam to width of the column expressed in terms of the yielding strength of rebar and the compressive strength of concrete, the limitation of the input shear for avoiding shear failure of the joint after flexural yielding of the beam, and the minimum amount of lateral reinforcement in the joint.

Shear transfer mechanism in the joint has been explained by the macroscopic model based on the strut failure mechanism by Paulay et al.[5]. On the other hand, from reappraisal of the existing test data and verification test, Shiohara et al. [6][7] indicated that the joint shear does not decrease or it may increase although the story shear degrades. They also pointed out that the above phenomena could not be explained by the macroscopic model based on the strut failure mechanism. Furthermore, they proposed a new macroscopic model for the joint shear failure including anchorage capacity of the beam rebars and investigated an effect of the anchorage capacity on failure mode and strength of the joint.

Shear failure in the joints is extremely complicated, and thus no consensus among researchers may be obtained on failure mode and resistant mechanism of the joints. On the other hand, a numerical procedure such as FEM is a very promising tool, because it provides detailed information such as internal stresses and strains for understanding failure mode, resistant mechanism and deformation capability of the joint. It is also easy to investigate effect of various parameters, provided that an analytical procedure used is shown to be reliable.

The RC interior beam-column joint specimens failing in shear in the joint tested by Kitayama et al.[8] are selected as a benchmark for the analysis. The nonlinear FE analyses are carried out especially by paying attention to: (1) spatial discretization; 2-D or 3-D, (2) type of the bond models; bond-slip or bond-locking model, and (3) type of the loading; monotonic or cyclic. The predicted failure modes and load-deflection curves are compared with the observed ones. Furthermore, Shiohara's macroscopic model [9], which is representative of the macroscopic models for describing the shear failure and resistant mechanism of the joint, is reviewed and validity of their hypotheses is rigorously investigated using the numerical results.

TEST PROGRAM

Kitayama et al. [8] conducted the cyclic lateral loading test on four scaled 1/2 interior beam-column joint assemblages. The major test variable was bond properties of longitudinal bars in the beam and column through the joint. The configuration and reinforcement detail are shown in Fig. 1. The test variables are listed in Table 1. The configuration is common to all specimens; a cross section of the columns is 350 mm x 350 mm and a cross section of the beams is 250 mm x 380 mm. Sixteen D22 rebars; deformed bar with a nominal diameter of 22 mm, are used in the column and four D25 rebars are used for both the top and bottom parts in the beam. The specimen referred to as "PBU-4" is a major target for this numerical study. Note that the amount of beam rebars in the joint was increased double of the beam rebars outside the joint. Besides PBU-4, the specimen referred to as "PNB-2", in which bond between the beam rebar in the joint and concrete is isolated, is also analyzed to investigate an effect of bond properties. The mechanical properties of concrete and reinforcing bars are indicated in Tables 2 and 3, respectively. The top and bottom ends of the column were pin-supported and both the ends of beam were roller-supported as the boundary condition. First, a constant axial load of 883 kN was applied to the top of the column, and then alternative cyclic lateral load was applied to the top of the column in an incremental fashion while keeping the axial load constant.

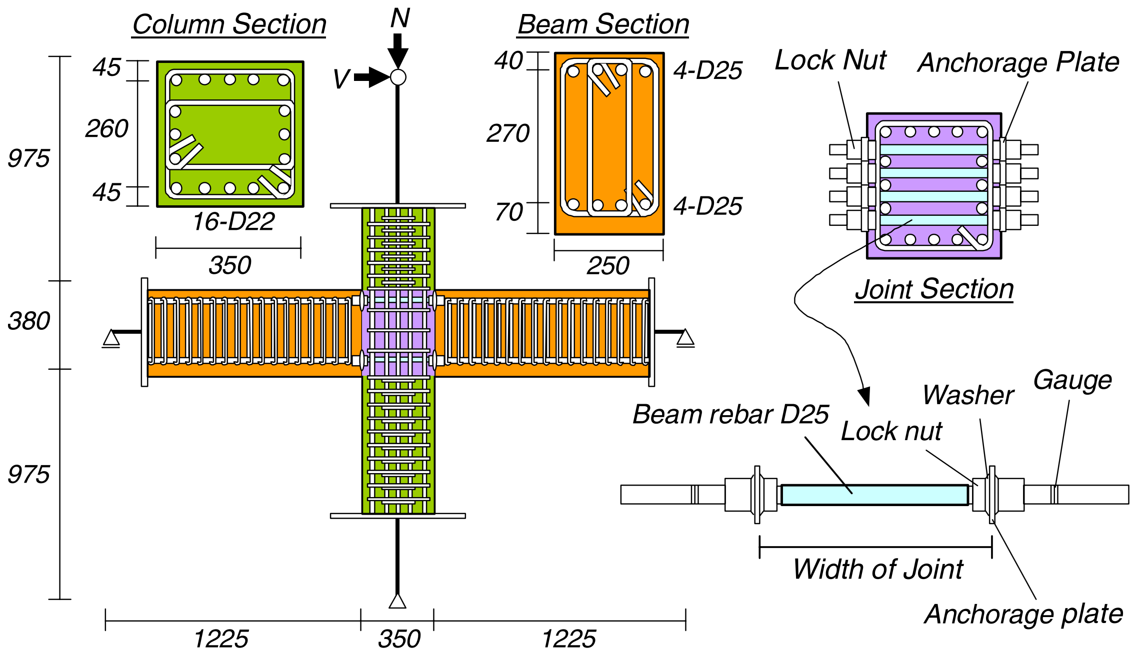

Figure 1 Configuration and reinforcement detail of beam-column joint specimen

Table 1 Test variables of beam-column joint specimens

Name of Specimen		PB-1	PNB-2	PNB-3	PBU-4
Applied Axial Force		Constant Compressive Force: 833 kN			
Rebar in Column		16-D22			
Rebar in Beam		Top Rebar: 4-D25 Bottom Rebar: 4-D25			
Reinforcement in Joint		2-D10@60 3 sets			
Anchorage Plate		used	used	used	not used
Bond in Joint	Beam Rebar	with bond	no bond	no bond	with bond
	Column Rebar	with bond	with bond	no bond	with bond

Table 2 Mechanical properties of concrete

Name of Specimen	Compressive Strength (MPa)	Tensile Strength (MPa)	Young's Modulus (GPa)
PB-1	21.0	2.1	25.1
PNB-2	21.0	2.4	25.7
PNB-3	21.9	2.1	26.0
PBU-4	22.2	2.4	25.8

Table 3 Mechanical properties of reinforcing bars

Reinforcing Bar	Yield Strength (MPa)	Tensile Strength (MPa)	Young's Modulus (GPa)
D10	404	629	175
D22	517	674	196
D25	534	685	191

FINITE ELEMENT MODELING OF SPECIMEN

Finite Element Discretization of Specimen

In order to investigate an effect of the spatial discretization, the beam-column joint specimen is divided by either 2-D mesh assuming plane stress state or 3-D mesh as shown in Fig. 2. Note that the mesh divisions for 2-D and 3-D are same in X-Y plane. Concrete is modeled by the four-node isoparametric quadrilateral element in 2-D discretization, and it is modeld by the eight-node solid element in 3-D discretization. Longitudinal bars in the beam and column are modeled by the discrete truss element to include an interaction between reinforcing bar and concrete. This interaction is modeled by introducing interface and/or linkage element(s) in the interface between truss element and concrete element. All other reinforcing bars are modeled by an embedded element, assuming perfect bond.

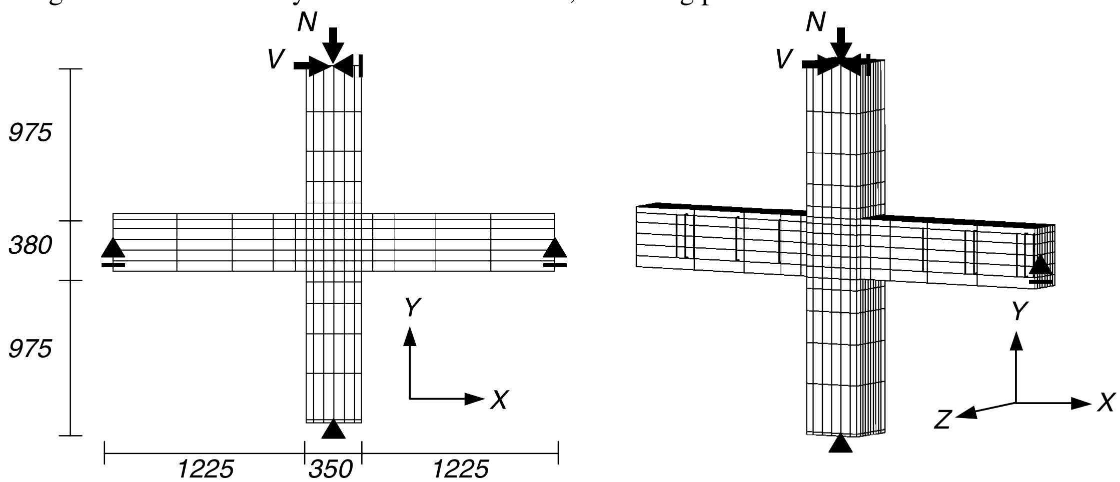

a. *2-D Discretization* b. *3-D Discretization*

Figure 2 Finite element mesh division

Constitutive Modeling of Reinforced Concrete

Modeling of concrete

Concrete is assumed to be a linear elastic continuum until crack occurs under tension or inelastic behavior starts with under compression. Cracking is judged according to the tension cut-off criterion. Constitutive law for cracked concrete is formulated based on the concept of so-called "decomposed-strain smeared crack model" by de Borst and Nauta [10]. Total strain, ε, is given as the sum of strain in the cracking part (refers to as "crack strain"), ε^{cr}, and strain in the solid part between cracks (refers to as "solid strain"), ε^{co}, as follows:

$$\varepsilon = \varepsilon^{cr} + \varepsilon^{co} = \varepsilon^{cr} + \varepsilon^{ce} + \varepsilon^{cp} \tag{1}$$

where ε^{ce} and ε^{cr} are the elastic and plastic components of the solid strain, respectively. This strain decomposition allows us to apply plasticity-based constitutive law for describing nonlinear behavior under compressive stresses. Elasto-plastic model based on Drucker-Prager criterion along with with an associated flow rule is used in the present study.

First, consider concrete with a single crack in a certain orientation. Here, 2-D constitutive law is formulated, since an extension of this to 3-D is straightforward. Provided that stress and deformation states in the cracking interface is given as shown in Fig. 3, relation between stresses and relative displacements is written as follows:

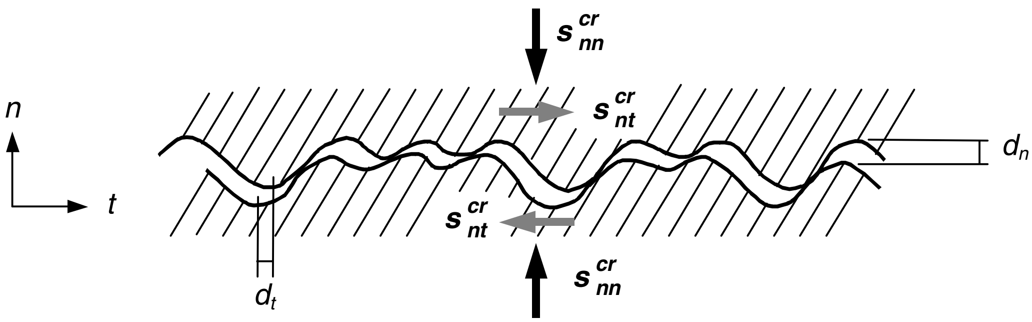

Figure 3 Sates in crack interface

$$\{d\sigma\}=[B]\{d\delta\} \quad or \quad \begin{Bmatrix} d\sigma_{nn}^{c} \\ d\sigma_{nt}^{c} \end{Bmatrix} = \begin{bmatrix} B_{nn} & B_{nt} \\ B_{tn} & B_{tt} \end{bmatrix} \begin{Bmatrix} d\delta_n \\ d\delta_t \end{Bmatrix} \tag{2}$$

where σ_{nn}^{c} and σ_{nt}^{c} are the normal and shear stresses, B_{nn}, B_{nt}, B_{tn} and B_{tt} are the material stiffness coefficients in the cracking part, and δ_n and δ_t are the crack width and slip displacement. Defining $d\varepsilon_{nn}^{cr} = d\delta_n/S$ and $d\gamma_{nt}^{cr} = d\delta_n/S$ with an average crack spacing S, then Eq.(2) can be rewritten in a form applicable to the constitutive law for the smeared crack model as follows:

$$\{d\sigma\}=\left[D^{cr}\right]\left\{d\varepsilon^{cr}\right\} \quad or \quad \begin{Bmatrix} d\sigma_{nn}^{c} \\ d\sigma_{nt}^{c} \end{Bmatrix} = \begin{bmatrix} S\cdot B_{nn} & S\cdot B_{nt} \\ S\cdot B_{tn} & S\cdot Btt \end{bmatrix} \begin{Bmatrix} d\varepsilon_{nn}^{cr} \\ d\gamma_{nt}^{cr} \end{Bmatrix} = \begin{bmatrix} D_{nn}^{cr} & D_{nt}^{cr} \\ D_{tn}^{cr} & D_{tt}^{cr} \end{bmatrix} \begin{Bmatrix} d\varepsilon_{nn}^{cr} \\ d\gamma_{nt}^{cr} \end{Bmatrix} \tag{3}$$

For simplicity, the off-diagonal terms in Eq.(3) is ignored; that is, $D_{nt}^{cr} = D_{tn}^{cr} = 0$. Finally, relation between the total stress increment $\{d\sigma\}$ and the total strain increment $\{d\varepsilon\}$ in the total coordinate system for cracked concrete can be written as follows according to de Borst and Nauta[9] and Rots[11]:

$$\{d\sigma\}=\left[\left[D_{ep}\right]-\left[D_{ep}\right][N]\left[\left[D^{cr}\right]+[N]^{T}\left[D_{ep}\right][N]\right]^{-1}[N]^{T}\left[D_{ep}\right]\right]\{d\varepsilon\} \tag{4}$$

where $[D_{ep}]$ is the elastic or elasto-plastic material stiffness of the solid concrete, and $[N]$ is the transformation matrix of crack. Multiple cracks with different directions may occur in RC structures subjected to cyclic loading. To cope with this difficulty, concept of the so-called “multi-directional fixed smeared crack model” by de Borst and Nauta[10] and Rots[11] is applied in this study.

In a specific application, it is important how the stiffness coefficients D_{nn}^{cr} and D_{tt}^{cr} in Eq.(3) are determined. D_{nn}^{cr} is defined by the secant stiffness normal to crack and D_{tt}^{cr} by the secant shear stiffness in the cracking part; that is, the former is determined on the basis of the tension softening curve and the latter is determined on the basis of the shear retention factor as follows:

$$D_{nn}^{cr} = \frac{\mu}{1-\mu}\cdot E \qquad D_{tt}^{cr} = \frac{\beta}{1-\beta}\cdot G \tag{5}$$

where E and G are the Young’s modulus and the elastic shear modulus of concrete, μ and β are the reduction factor of Young’s modulus and the shear reduction factor.

Modeling of interaction between reinforcing bar and concrete

It is known that stresses in the interface between reinforcing bar and concrete are transferred by cohesive action, frictional action and locking action between protrusion of deformed bar and concrete. Many past studies simply modeled bond behavior induced by these interactions as bond stress (τ_b) - slip (Δ_s) relation. Trilinear τ_s - Δ_s model constructed by modifying the so-called "Kaku model" has been frequently used in FE applications of the beam-column joints by Sugaya and Owada[12] and Noguchi et al.[13]. The modified Kaku model and CEB model [14] as shown in Fig. 4 are used as τ_b - Δ_s relation and they are represented by the interface element. In order to include the locking action of protrusion in 3-D analysis, bond behavior of the steel part between protrusions is represented by τ_b - Δ_s model for the round smooth bar provided by the CEB model code and the locking action is modeled by the linkage element consisting of a set of inclined orthogonal springs as shown in Fig. 5. The inclined springs have compressive resistance but no tensile resistance. The axial compressive stiffness of spring, K_w, is determined according to the following equation by Fujii[15]:

$$K_w = \frac{\pi \cdot (d+\ell) \cdot L \cdot E_c \cdot \cos 2\theta}{\ell} \tag{6}$$

where d is the diameter of reinforcing bar, L is the bar length covered by a set of springs, ℓ is the length of local deformation zone and is assumed to be equal to $d/20$, θ is the angle between the bar axis and the spring direction and is assumed to be $45°$, and E_c is the Young's modulus of concrete. Note that the linkage element for the beam or column rebar is allocated in the X-Z or Y-Z plane of the beam-column joint.

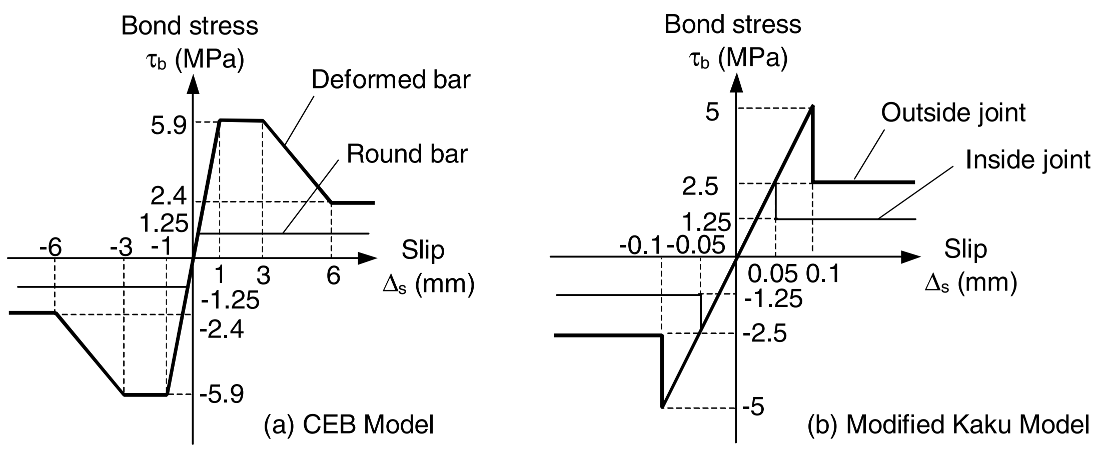

Figure 4 Assumed bond stress-slip models for deformed and round bars

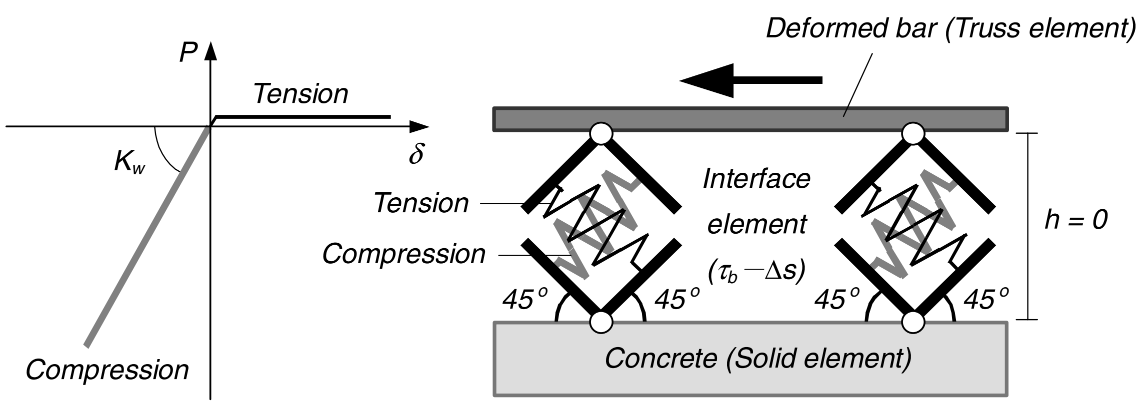

Figure 5 Bond-locking Model

Material Modeling

Uniaxial stress-strain relation for concrete under tension is assumed to be linear elastic up to its tensile strength, f_t. Descending branch after cracking is represented by a tril-inear tension softening curve with fracture energy as shown in Fig. 6. The fracture energy of concrete, G_F (N/mm^2), is determined by the formula by Oh-oka et al.[16]:

$$G_F = \frac{0.23 f_c + 136}{1000} \tag{7}$$

where f_c is the compressive strength of concrete (N/mm^2). In order to minimize localization of the fracture, the crack strain, ε^{cr}, is defined by dividing the crack width, W, by characteristic element length, L_c for regularization: $\varepsilon^{cr} = W/L_c$. The characteristic length for 2-D problem is defined as a diameter of a circle with an equivalent area to the element area, A, and L_c for 3-D problem is defined as a diameter of a sphere with an equivalent volume to the element volume, V. Note that the origin-oriented secant stiffness is assumed for unloading and reloading.

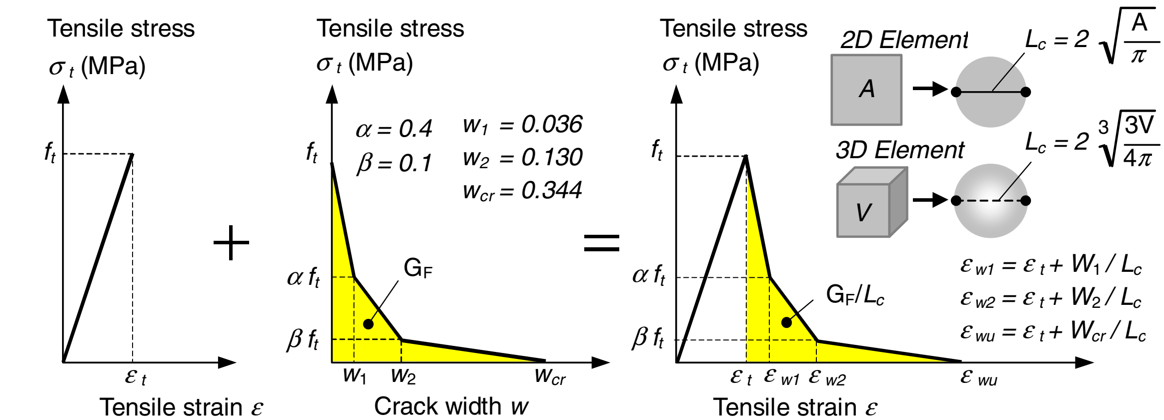

Figure 6 Uniaxial tensile stress-strain relationship for concrete

Uniaxial stress-strain relation of concrete under compression up to the compressive strength, f_c, is represented by a bilinear model with an intersection point at f_c /3 as shown in Fig. 7. The descending branch after the peak is represented by a linear compressive strain softening model with compressive fracture energy, G_{FC} (N/mm). The compressive fracture energy is determined according to the formula by Nakamura and Higai[17]:

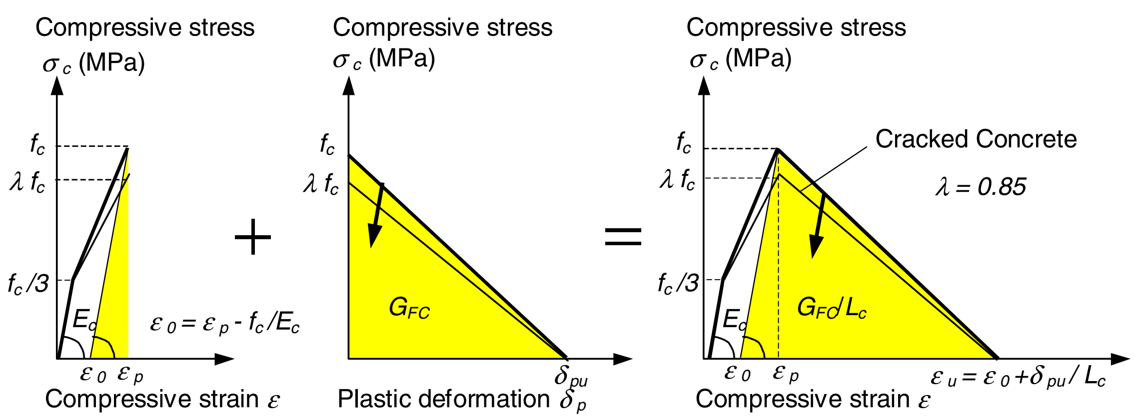

Figure 7 Uniaxial compressive stress-strain relationship for concrete

$$G_{FC} = 8.8\sqrt{f_c} \tag{8}$$

The plastic strain in the solid concrete, ε^{cp}, is defined by dividing the plastic deformation, δ_p, by the characteristic element length, L_c, for regularization. The definition of characteristic element length for compression is similar to that for tension. Compressive strength reduction factor, λ, is introduced to take compressive softening of the cracked concrete into consideration, and λ is assumed to be 0.85 in this study. The shear retention factor for the cracked concrete, β, is determined as a ratio of the shear stiffness of the cracked concrete, G^{cr}, to the elastic shear modulus of concrete, G^{co}, according to the formula by Walraven and Kauser[18]:

$$\beta = G^{cr} / G^{co} = \frac{1}{1 + 4447 \cdot \varepsilon^{cr}} \tag{9}$$

The assumed uniaxial stress-strain relations of concrete and reinforcing bar are shown in Fig. 8. Reinforcing bar is treated as an elasto-plastic material and its constitutive law is derived on the basis of the von-Mises yield criterion. Gradient after yielding is 1/100 of the initial stiffness, E_s.

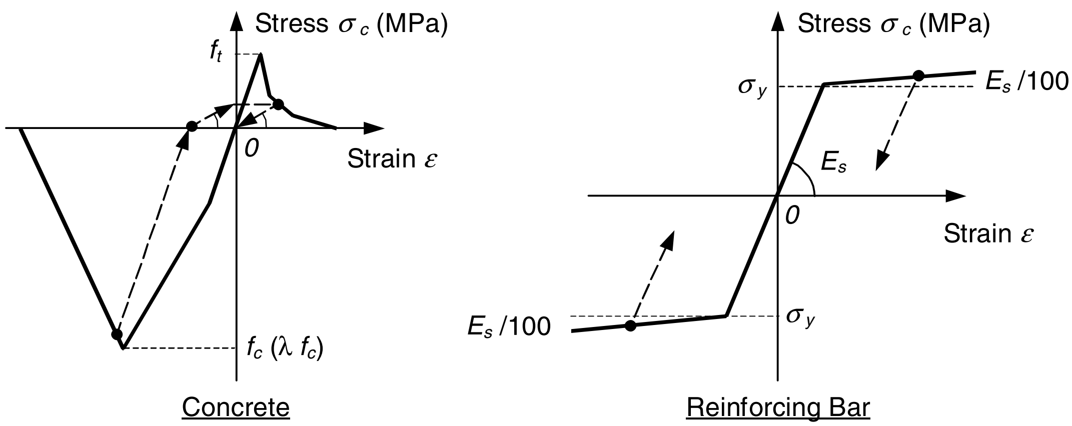

Figure 8 Uniaxial stress-strain relation of concrete and reinforcing bar

RESULTS AND DISSCUSSION

Numerical Results

Analytical model and parameters

Adopted analytical models are listed in Table 4. The numerical analyses of the beam-column joint specimens are performed using four kinds of models with a different combination of parameters: spatial discretization (2-D or 3-D), bond model (bond slip model or bond locking model) and compressive strength reduction factor of concrete (λ = 1.0 or 0.85). First, constant axial load is applied to the top of the column, and then lateral load is applied to the top of the column incrementally by the displacement control. An internal friction angle of concrete, ϕ, was set equal to 10° in 3-D analysis. On the other hand, ϕ for 2-D analysis was set equal to $35^{o,}$ which gives comparable response to 3-D response. DIANA-7.2 [19] was used as the computer code in the present study.

Table 4 Analytical models and parameter

Type of Model	Discretization	Bond Model	Comp. Strength Reduction Factor
Model-I	2-D	CEB Model	$\lambda = 1.00$
Model-II (2)	2-D	CEB Model	
Model-II (3)	3-D	CEB Model	
Model-III (2)	2-D	Modified Kaku Model	$\lambda = 0.85$
Model-IV (3)	3-D	Bond Locking Model	
Model-V (3)	3-D	No Bond	

Story shear versus story drift angle relations by monotonic loading analysis

Fig. 9 compares the calculated story shear (V)-story drift angle (R) relation with the test one for the specimen of PBU-4. First, Fig. 9(a) shows effect of the compressive strength reduction factor on response by 2-D analysis. Model-I(2) gives a similar initial stiffness to the test, but it overestimates the ultimate strength. On the other hand, Model-II(2) and Model-III(2) give relatively good predictions to the observed initial stiffness and ultimate strength. As far as PBU-4 is concerned, effect of the compressive softening of the cracked concrete is more significant than that of the bond model on capacity of the specimen. Fig. 9(b) compares the calculated V–R relations by 2-D analysis using Model-II(2) and 3-D analyses using Model-II(3) and Model-IV(3) with the observed one for PBU-4. The calculated results by all the analyses are in good agreement with the test one until the story drift angle, R, reaches R = 1/50, which corresponds to the ultimate strength of the specimen. 2-D analysis can simulate the observed post-peak behavior. On the other hand, both the 3-D analyses slightly overestimate the post-peak shear resistance of the beam-column joint. It seems that 2-D analysis gives better response prediction of the beam-column joint than 3-D analysis. However, it must be noted that these results are obtained under the condition of the monotonic loading and thus cyclic deterioration is not taken into account.

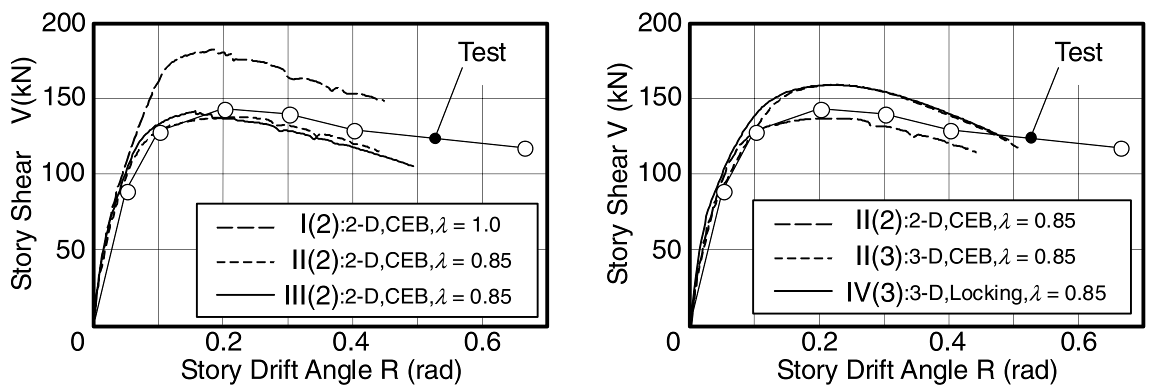

(a) Compressive strength reduction factor (b) spatial discretization

Figure 9 Story shear-story drift angle relation

Story shear versus story drift angle relations by cyclic loading analysis

Fig. 10 compares the calculated cyclic story shear-story drift angle relations obtained by 2-D analysis using Model-II(2) and 3-D analysis using Model-IV(3) with the observed one for PBU-4. Although 2-D analysis could well simulate V-R response under the monotonic loading, it gives the hysteresis loop of spindle-type, which is quite different from the observed hysteresis loop of slip-type. On the other hand, 3-D analysis gives much better prediction than 2-D analysis, because it can reproduce cyclic deterioration after the peak and the hysteresis loop of slip-type as observed in the test. Thus, the bond-locking model is effective to investigate failure mode and post-peak behavior of the beam-column joint.

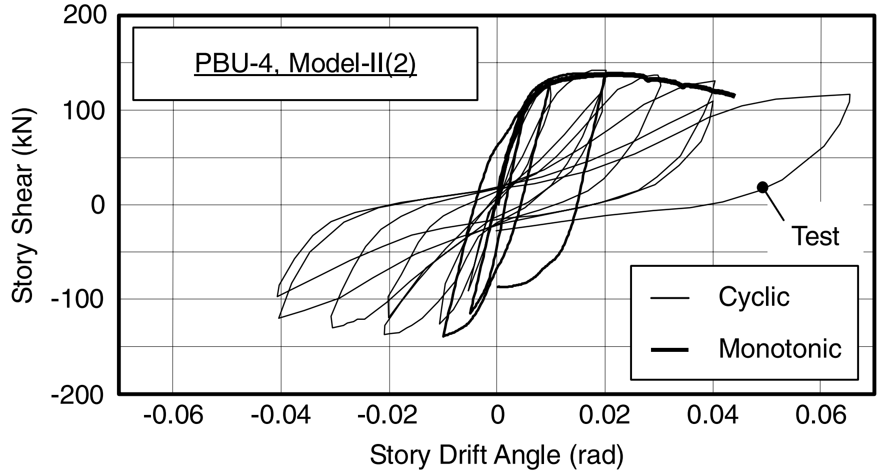

(a) 2-D Analysis

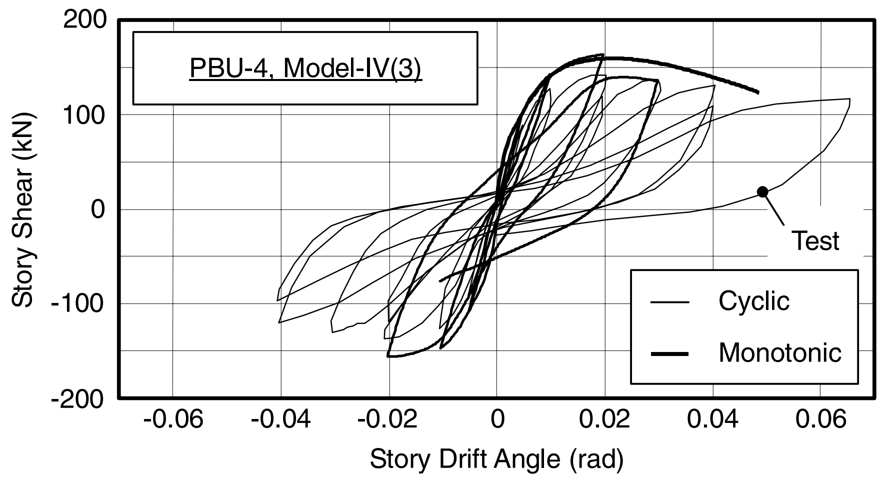

(b) 3-D Analysis

Figure 10 Story shear versus story drift angle relation

Damage distributions in terms of principal strains in concrete

Fig. 11 shows the maximum and minimum principal strain distributions in concrete at R = 1/50 for PBU-4 obtained by using Model-II(2) and Model- IV(3) under cyclic loading. Darker a color, larger tensile strain; that is, dark region indicates crack-induced damage zone and light region indicates zone with compressive or smaller tensile strain. The damage zones by 2-D are observed in the joint and at the ends of beams and columns. On the other hand, the damage zones by 3-D are observed only in the joint and at the ends of beams. The damage in the joint obtained by 2-D is larger in magnitude and wider in area than that by 3-D. The minimum principal strains in the joint by 2-D are in a compressive state and are widely distributed over the joint; forming a mechanism of diagonal compression strut. On the other hand, magnitude of the minimum principal strains in the joint by 3-D is small and they are almost in a tensile state; forming a weak diagonal tension strut.

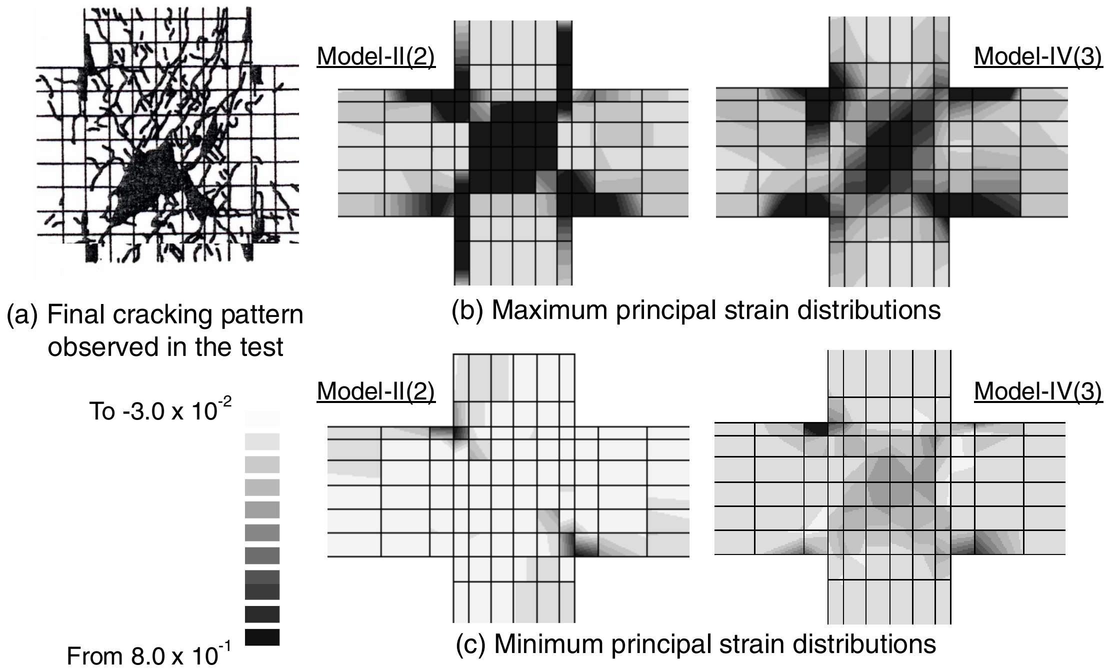

Figure 11 Maximum and minimum principal strain distributions

Shear Resistant Mechanism of Joint

Shiohara's macrscopic model

Fig. 12 demonstrates a schematic diagram of the resistant mechanism for the joint failing in shear proposed by shiohara et al. The hypotheses made by Shiohara[6][7] for constructing a macroscopic model are summarized as follows:

(1) Even if story shear of the beam-column joint assemblage decreases after the peak, shear taken by the joint may not decrease but even increase.

(2) Transition of the compressive axial force in the beam rebar in the compression side at the beam end section to the tensile axial force may occur due to bond deterioration. Now, this compressive force in the beam rebar will be taken by concrete in the compression side and this leads to an expansion of the compressive region, resulting in shift of position of the compressive stress resultant of concrete toward center of the beam section; that is, flexural resistance will be reduced because lever arm between the stress resultants in the beam section is reduced.

(3) Post-peak degradation in the story shear V will be not caused by failure of the shear resistant mechanism but by failure of the moment resistant mechanism in the joint.

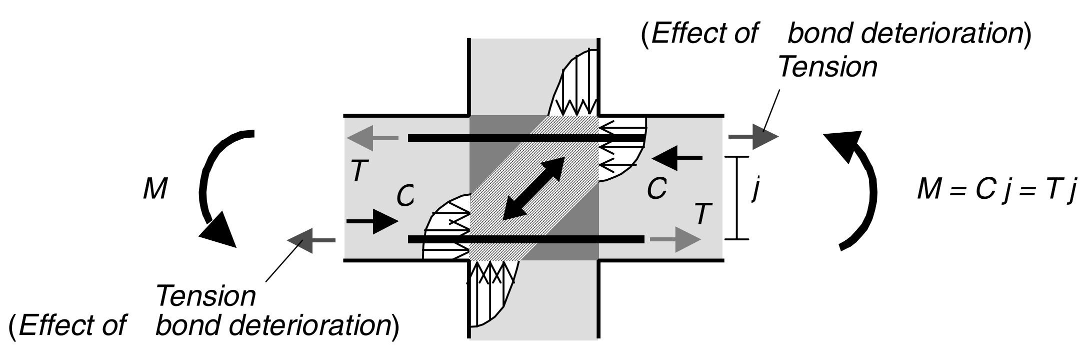

Figure 12 Shear resistant mechanism

Joint shear stress versus story drift angle relation

Fig. 13 compares the calculated joint shear stress (τ_j)-story drift angle (R) relation by Model-IV(3) with the test one for PBU-4. For comparison, the calculated τ_j - R relation by Model-V(3) for PNB-2 is also shown in the figure. The joint shear stress, τ_j, is determined by dividing the joint shear, V_j, by an effective area of the joint, A_{eff} [20]. The joint shear, V_j, is calculated by the following equation:

$$V_j = \sum a_t \sigma_s + \sum a_t' \sigma_s' - V \tag{10}$$

where a_t and a'_t are the areas of tensile steel bars in the beam at both sides of the joint, σ_t and σ'_t are the tensile steel stresses, and V is the story shear. It is seen from Fig. 13 that the calculated shear stresses in the joint for PBU-4 and PNB-2 do not decrease with an increase in R as well as the observed results. This supports validity of the hypothesis (1) by Shiohara et al.

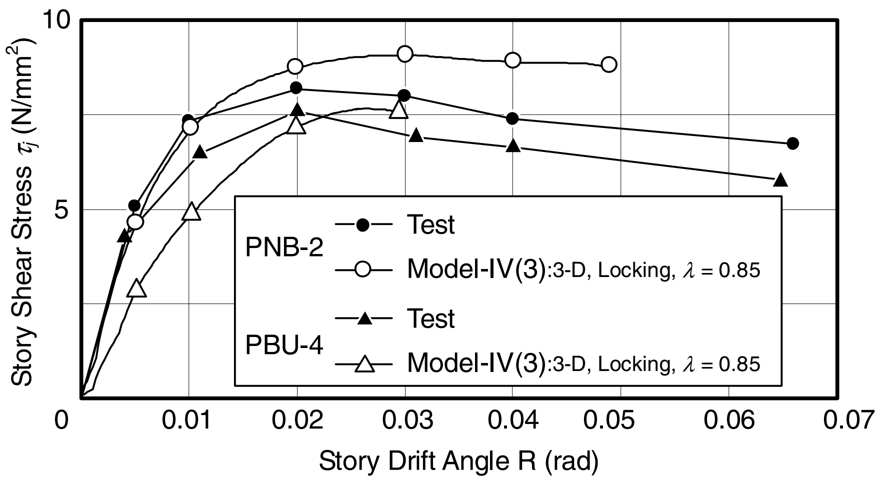

Figure 13 Joint shear stress versus story drift angle relation

Stress distribution of concrete and reinforcing bars at beam end

Figures 14 and 15 show the longitudinal stress distributions of concrete and beam rebars along the cross section at the beam end obtained by using Model-II(2) and Model-IV(3) under cyclic loading when R = 1/50. The stress distributions of concrete by 3-D analysis are different from that by 2-D analysis. Compressive stresses by 2-D analysis are gradually decreasing from the maximum value at the top to zero value nearby the bottom bar, except for the region just below the top bar with a sudden stress drop. In case of 3-D analysis, the maximum compressive stress for the central section is located at the top part and it exceeds the compressive strength of concrete due to the confinement effect of reinforcing bars. On the other hand, the maximum compressive stress for the section along side cover concrete is located in the lower part of the top rebar and strain softening occurs in the top cover concrete. Compressive stresses are abruptly decreasing zero value nearby a center of the beam section. Now, look at the stress distribution of reinforcing bars. Magnitudes of the tensile stresses in the top and bottom rebars by 2-D analysis are larger than those by 3-D analysis. It is interesting to note that stresses in the top by 2-D and 3-D analyses turn out to be tension instead of compression. Fig. 16 shows the observed and calculated strain distribution of the bottom bar through the joint when R = 1/50. It is seen that the tensile stresses are caused in the bottom bar in the compression side at the beam end, although a complete agreement in the strain distributions along the bar for the test and analysis is not attained. These stress and strain distributions support validity of the hypothesis of (2) by Shiohara et al.

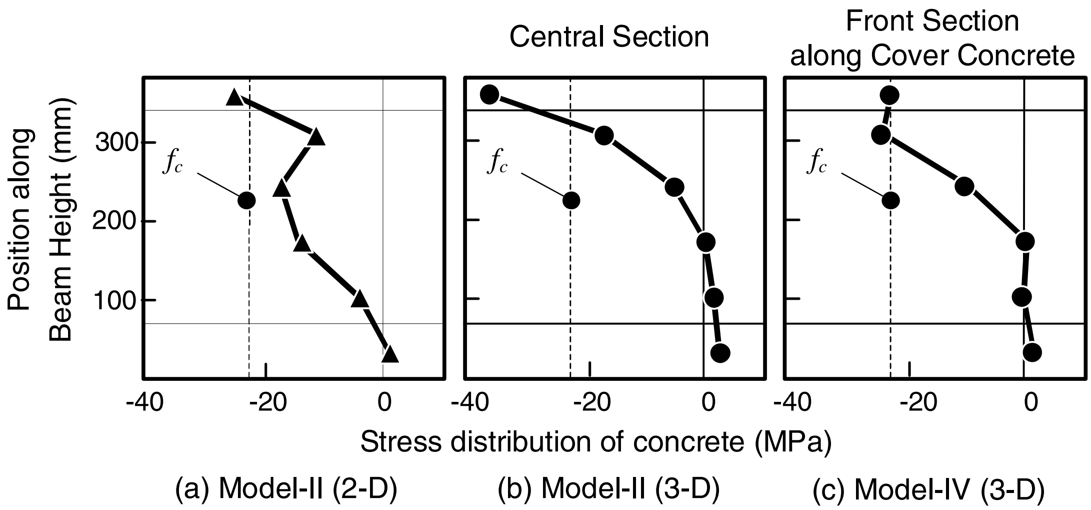

Figure 14 Longitudinal stress distributions of concrete along beam height

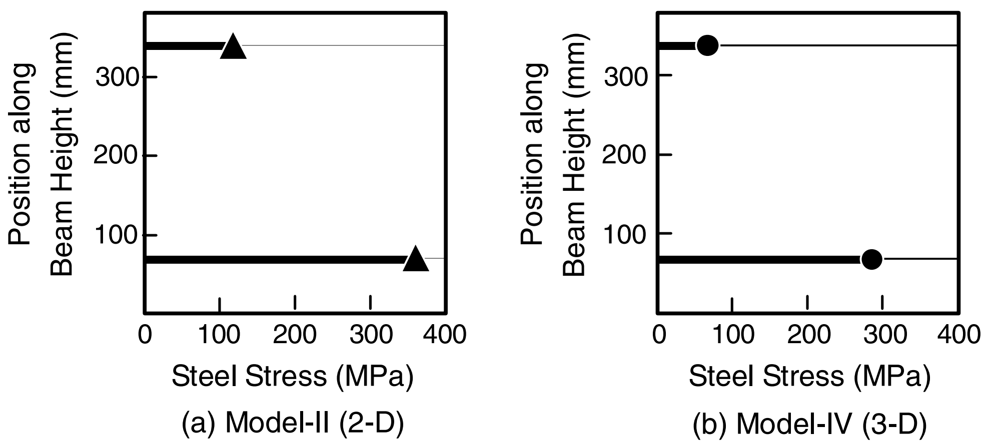

Figure 15 Stress distributions of reinforcing bar along beam height

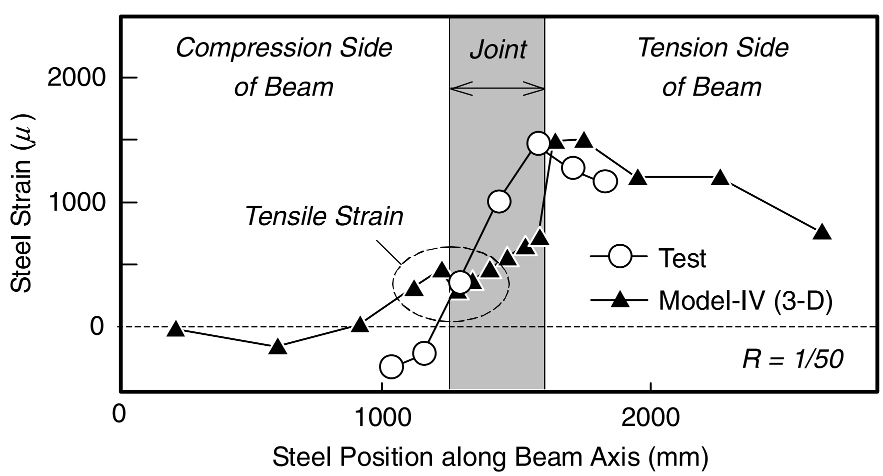

Figure 16 Strain distributions of bottom bar in beam along beam axis

Variation in lever arm between stress resultants

Fig. 17 compares the calculated lever arm (j) versus story drift angle (R) relation obtained using Model-IV(3) with the observed one. The lever arm j for Case-1 is calculated by dividing the beam end moment by the axial force in the tension bar, and j for Case-2 is determined with all stress resultants of concrete and bar elements located at the beam end. The calculated values for Case-1 and Case-2 show a similar tendency to the test one; j decreases with an increase in R, supporting validity of the hypothesis of (3) by Shiohara et al.

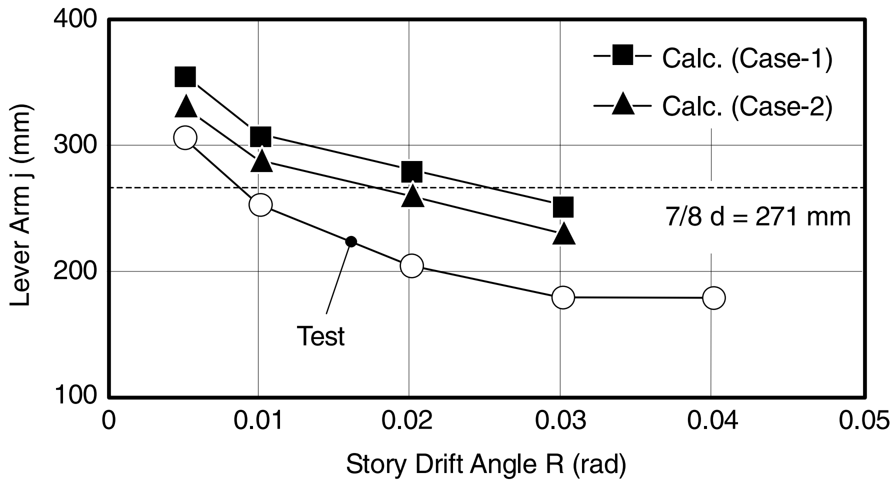

Figure 17 Variation in lever arm with increase in story drift angle

CONCLUSIONS

In the present study, the RC beam-column joint specimens failing in joint shear were analyzed by the nonlinear FEM, especially paying attention to the spatial discretization, the bond model and the loading type. The failure mode and post-peak behaviors including shear resistant mechanism and cyclic deterioration of the joint were investigated and the following findings were obtained:

(1) 2-D analysis, which takes the compression softening and bond-slip behavior into account, gives comparable story shear-story drift angle relation to the observed ones under the monotonic loading condition. However, it provides the hysteresis loop of spindle-type under the cyclic loading, which is different from that of slip-type observed in the test.

(2) 3-D analysis, which takes the bond-locking action into account as well as the compression softening, is able to reproduce cyclic deterioration and hysteresis loop after the peak load fairly well, although it slightly overestimates the shear capacity of the joint.

(3) It is possible to understand damage distribution in the joint by examining the maximum and minimum principal strain distributions. It seems that 3-D analysis gives better representation of the failure mode than the 2-D analysis.

(4) The present analysis can demonstrate validity of the Shiohara's hypotheses that reduction of the story shear after the peak load may come from failure of the moment-resistant mechanism.

ACKNOWLEDGEMENT

This research was conducted as part of the Academically Promoted Frontier Research on "Sustainable City Based on Environmental Preservation and Disaster Prevention" at Nihon University, College of Science and Technology (Head Investigator: Prof. Ohtsu) under A Grant from the Ministry of Education, Science, Sports and Culture. The authors express thier thanks to Mr. R. Ozaki (graduate student) for his contribution to the numerical work.

REFERENCES

1. American Concrete Institute (ACI). "Building code requirement for structural concrete and commentary". Farmington Hills, Michigan. ACI 318-95. 1995.
2. Architectural Institute of Japan (AIJ). "AIJ structural design guidelines for reinforced concrete buildings". Tokyo, Japan, 1994. (in Japanese)
3. Standard Association of New Zealand (SANZ). "Concrete structure standard: part 1: the design of concrete structures". NZS 3101, Wellington, New Zealand, 1995.
4. Kitayama K, Otani S, and Aoyama H. "Earthquake resistant design criteria for reinforced concrete interior beam-column joints". Proceedings of Pacific Conference on Earthquake Engineering, Wairakei, New Zealand. Vol.1. 315-326. 1987.
5. Paulay T, Park R, and Priestly M N. "Reinforced concrete beam-column joints under seismic actions". ACI Journal. 585-593. 1978.
6. Kusuhara F, Shiohara H. "Re-evaluation of joint shear tests of R/C beam-column joint failed in shear". Proceedings of the Japan Concrete Institute. Vol.19. No.2. 1005-1010. 1997. (in Japanese)
7. Kishikawa S, Shiohara H. "Relation of joint shear and joint shear failure in reinforced concrete beam-column joint". Proceedings of the Japan Concrete Institute. Vol.20. No.3. 523-528. 1998. (in Japanese)
8. Tajima Y, Kitayama K, Okuda M, and Kishida S. "Influences of beam and column bar bond on failure mechanism in reinforced concrete interior beam-column joints". Proceedings of the Japan Concrete Institute. No.3. 697-702. 2000. (in Japanese)
9. Shiohara H. "New model for shear failure of RC interior beam-column connections". Journal of Structural Engineering. ASCE. 127(2). 152-160. 2001.
10. De Borst R, Nauta P. "Non-orthogonal cracks in a smeared finite element model". Engineering Computations. 2. 35-46. 1985.
11. Rots J G. "Computational modeling of concrete fracture". PhD thesis, Delft University of Technology. 1988.
12. Sugaya K, Owada Y. "Studies on non-linear behaviors of reinforced concrete beam-column joint under seismic load". Summaries of Technical Papers of Annual Meeting, AIJ, Structures IV. 669-670. 1996. (in Japanese)
13. Noguchi H, Zhnang D, and Kashiwazaki K. "Three-dimensional finite element analysis of RC beam-column joints reinforced by new reinforcing way". Proceedings of the Japan Concrete Institute. Vol.24. No.2. 397-402. 2002. (in Japanese)
14. CEB. "CEB-FIP model code". Thomas Telford Service Ltd.
15. Fujii S. "Bond anchorage properties in reinforced concrete and its influence on performance of reinforced concrete members". Doctoral Thesis, Kyoto University. 1992. (in Japanese)
16. Oh-oka T, Kitsutaka Y, and Watanabe K. "Influence of short cut fiber mixing and curing time on the fracture parameter of concrete". Journal of Structural and Construction Engineering, Transactions of AIJ. No.529. 1-6. 2000. (in Japanese)
17. Nakamura H, Higai T. "Compressive fracture energy and fracture zone length of Concrete, Modeling of Inelastic Behavior of RC Structures under Seismic Loads". ASCE. SEI. 471-487. 1999.
18. Walraven J C, Keuser W. "The shear retention factor as a compromise between numerical simplicity and realistic material behavior". Darmstadt Concrete. 2. 221-234. 1987
19. DIANA Foundation Expertise Center for Computational Mechanics. "DIANA finite element analysis user's manual". TNO Building and Construction Research. 1999.
20. AIJ. "Design guidelines for earthquake resistant reinforced concrete buildings based on ultimate strength concept". Tokyo, Japan. 1990. (in Japanese)